

# Essential structural profile of a dual functional inhibitor against cyclooxygenase-2 (COX-2) and 5-lipoxygenase (5-LOX): Molecular docking and 3D-QSAR analyses on DHDMBF analogues

Mingyue Zheng, Zhenshan Zhang, Weiliang Zhu,\* Hong Liu,\* Xiaomin Luo, Kaixian Chen and Hualiang Jiang\*

*Drug Discovery and Design Center, State Key Laboratory of Drug Research, Shanghai Institute of Materia Medica, Shanghai Institutes for Biological Sciences, Chinese Academy of Sciences, Shanghai 201203, PR China*

Received 25 November 2005; revised 29 December 2005; accepted 30 December 2005

Available online 2 February 2006

**Abstract**—It is recently proposed that compounds with equal capabilities of inhibiting COX and 5-LOX, both are key enzymes involved in the arachidonic acid (AA) cascade, are expected to be safer non-steroidal anti-inflammatory drugs (NSAIDs). To dig out helpful information in designing dual functional inhibitors against the two enzymes, homology modeling, molecular dynamics (MD) simulations, automated docking, and 3D-QSAR analyses were performed in this study on 21 COX-2/5-LOX dual inhibitors, namely, 7-*tert*-butyl-2,3-dihydro-3,3-dimethylbenzofuran (DHDMBF) analogues. A 3D-model of 5-LOX was built based on the high-resolution X-ray structure of rabbit reticulocyte 15-lipoxygenase. Molecular docking was then applied to locate the binding orientations and conformations of DHDMBF analogues with COX-2 and 5-LOX, respectively, leading to highly predictive CoMFA models constructed on the basis of the binding conformations with  $q^2$  values of 0.782 and 0.634 for COX-2 and 5-LOX, respectively. In addition, CoMFA field distributions were found in good agreement with the structural characteristics of the corresponding binding sites. Both the docking simulations and QSAR analyses suggest that new potent dual inhibitors should share a structural feature with a moderately bulky group at R<sub>2</sub> position and a rather negatively charged group around the position of the carbonyl group of DHDMBFs. Therefore, the final 3D-QSAR models and the information of the inhibitor–enzyme interaction should be useful in developing new NSAIDs as anti-inflammation drugs with favorable safety profile.

© 2006 Elsevier Ltd. All rights reserved.

## 1. Introduction

The withdrawal of rofecoxib (Vioxx) in 2004 aroused public concerns about the safety of non-steroidal anti-inflammatory drugs (NSAIDs) that formed the mainstay in the treatment of inflammatory disease.<sup>1</sup> The action mechanism of the drug is to inhibit cyclooxygenases (COXs), which are involved in the formation of prostaglandins and thromboxanes from arachidonic acid (AA) in cellular membranes.<sup>2,3</sup> However, it has been pointed out that inhibiting COX pathway could shunt the metabolism of AA toward the 5-lipoxygenase (5-LOX) pathway,<sup>4</sup> increasing the formation of leukotri-

enes, leading to inflammation and NSAIDs-induced adverse effects, e.g., asthma and gastrointestinal damage that is the most troublesome side effect of NSAIDs.<sup>4–6</sup>

On the other hand, 5-LOX was found to play an etiological role in both cardiovascular and cerebrovascular diseases.<sup>5–7</sup> Products of the 5-LOX pathway, LTB<sub>4</sub> and LTE<sub>4</sub>, are detectable in atherosclerotic lesions.<sup>8,9,10</sup> Very recently, genetic studies have associated 5-LOX and its accessory protein, 5-LOX-activating protein, with cardiovascular disease, myocardial infarction, and stroke.<sup>7,11–13</sup> Lötzer et al. proposed a “5-LOX atherosclerosis hypothesis”<sup>14</sup> that further stresses the 5-LOX atherosclerosis connection. Combined with the earlier studies that COX inhibition alone leads to an up-regulation of AA metabolism by the 5-LOX pathway,<sup>15</sup> it is no more difficult to find out latent cardiovascular hazards of COX-2 selective NSAID. Therefore, it is expected that

**Keywords:** COX-2; 5-LOX; Dual inhibitor; NSAIDs; DHDMBF; Homology modeling; Docking; 3D-QSAR; CoMFA; CoMSIA.

\* Corresponding authors. Tel.: +86 21 50806600x1210; fax: +86 21 50807088; e-mail: [hlijiang@mail.shcnc.ac.cn](mailto:hlijiang@mail.shcnc.ac.cn)

dual inhibitors against both COX-2 and 5-LOX should present an enhanced anti-inflammatory potency without risks of serious side effects such as cardiovascular events. Indeed, combination of the inhibitors of COXs and of 5-LOX showed to be more effective than either class of drugs used alone.<sup>16</sup> Therefore, a single agent inhibiting both enzymes is of interest to medicinal chemistry.<sup>17</sup>

Several chemical families of dual COX-2/5-LOX inhibitors were reported,<sup>18,19</sup> one of which is 7-*tert*-butyl-2,3-dihydro-3,3-dimethylbenzofuran (DHDMBF) analogues (Table 1)<sup>20</sup> with analgesic efficacy and excellent gastric safety in a variety of in vivo tests.<sup>21–23</sup> In the present study, we constructed a three-dimensional (3D) model of the human 5-LOX receptor via homology modeling. Then, 27 DHDMBF analogues were docked to the binding site of COX-2 and the substrate-binding pocket of 5-LOX, respectively. Finally, the binding conformations of the compounds via molecular docking were used to construct 3D-QSAR models by comparative molecular field analysis (CoMFA)<sup>24</sup> and compara-

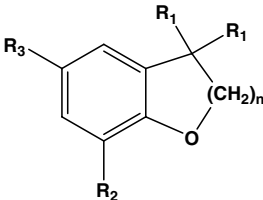
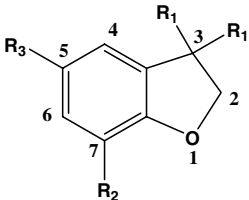
tive molecular similarity indices analysis (CoMSIA).<sup>24</sup> The aims of this study are: (i) to demonstrate the common binding model of DHDMBF analogues with COX-2/5-LOX, (ii) elucidate the structural features associated with the chemical modifications and explain the SAR data for dual inhibitors, and (iii) construct highly predictive QSAR models for designing novel potent NSAIDs with dual functions.

## 2. Computation details

### 2.1. Sequence alignment

In mammals, the N-terminal  $\beta$ -barrel domain of LOXs, consisting of around 120 amino acids, was found to be not essential for their catalytic activity.<sup>25</sup> To simplify the homology model and reduce the computational workload, these 120 residues were removed, to focus on the binding site of human 5-LOX.<sup>26</sup> Amino acid sequence of human 5-LOX was retrieved from

**Table 1.** Structures and in vitro COX-2/5-LOX inhibitory activities of 27 DHDMBF analogues and their predicted binding free energy (kcal/mol) to COX-2 and 5-LOX

<div><div></div><div>DHDMBF analogues</div></div>					<div><div></div><div>DHDMBFs</div></div>			
Compound	<i>n</i>	R <sub>1</sub>	R <sub>2</sub>	R <sub>3</sub>	COX-2		5-LOX	
					−log IC <sub>50</sub>	Δ <i>G</i> (kcal/mol)	−log IC <sub>50</sub>	Δ <i>G</i> (kcal/mol)
<b>1</b>	1	Me	<i>t</i> -Bu	CO(CH <sub>2</sub> ) <sub>3</sub> CCH	7.82	−11.41	5.22	−10.09
<b>2</b>	1	Me	<i>t</i> -Bu	COPr	7.02	−10.42	5.07	−10.34
<b>3</b>	1	Me	<i>t</i> -Bu	COPhenyl	8.15	−11.59	5.30	−10.16
<b>4</b>	1	Me	<i>t</i> -Bu	COBu	7.40	−10.82	4.92	−9.72
<b>5</b>	1	Me	<i>t</i> -Bu	CO(CH <sub>2</sub> ) <sub>3</sub> - <i>c</i> -Pr	6.66	−8.74	5.10	−10.12
<b>6</b>	1	Me	<i>t</i> -Bu	CO(CH <sub>2</sub> ) <sub>3</sub> CHMe <sub>2</sub>	5.35	−9.61	5.27	−10.47
<b>7</b>	1	Me	<i>t</i> -Bu	COCH <sub>2</sub> C(Cl)Me <sub>2</sub>	7.00	−10.19	5.10	−10.26
<b>8</b>	1	H	<i>t</i> -Bu	CO(CH <sub>2</sub> ) <sub>3</sub> - <i>c</i> -Pr	4.82	−9.18	4.92	−10.26
<b>9</b>	1	Me	Et	CO(CH <sub>2</sub> ) <sub>3</sub> - <i>c</i> -Pr	5.30	−8.32	4.74	−10.3
<b>10</b>	2	Me	<i>t</i> -Bu	CO(CH <sub>2</sub> ) <sub>3</sub> - <i>c</i> -Pr	5.52	−8.85	5.10	−10.08
<b>11</b>	1	Me	<i>t</i> -Bu	CONHPr	6.02	−9.42	4.30	−9.02
<b>12</b>	1	Me	<i>t</i> -Bu	CONH- <i>c</i> -Pr	6.26	−9.35	4.30	−9.14
<b>13</b>	1	Me	<i>t</i> -Bu	CONH(CH <sub>2</sub> ) <sub>2</sub> OMe	7.52	−9.94	4.30	−9.91
<b>14</b>	1	Me	<i>t</i> -Bu	CONMeEt	5.35	−8.24	4.66	−9.42
<b>15</b>	1	Me	<i>t</i> -Bu	CONMe- <i>c</i> -Pr	6.00	−7.71	4.92	−9.73
<b>16</b>	1	Me	<i>t</i> -Bu	NH(C <sub>3</sub> H <sub>5</sub> N <sub>2</sub> )	4.00	−7.56	5.12	−10.05
<b>17</b>	1	Me	<i>t</i> -Bu	2-Thienyl	7.15	−10.57	5.05	−9.84
<b>18</b>	1	Me	<i>t</i> -Bu	6-Imidazo[2.1- <i>b</i> ]thiazolyl	7.82	−11.94	5.00	−9.94
<b>19</b>	1	Me	<i>t</i> -Bu	3-Methylene- $\gamma$ -butyrolactonyl	7.46	−10.56	5.40	−10.5
<b>20</b>	1	Me	<i>t</i> -Bu	CO-2-thienyl	7.42	−10.97	5.00	−9.74
<b>21</b>	1	Me	<i>t</i> -Bu	( <i>E</i> )-CH=CH-2-thienyl	7.46	−9.84	5.22	−10.4
<b>22<sup>a</sup></b>	1	Me	<i>t</i> -Bu	COpentyl	7.05	−11.23	NT	
<b>23<sup>a</sup></b>	1	Me	<i>t</i> -Bu	CO- <i>E</i> -CH=CHCH <sub>2</sub> - <i>c</i> -Pr	6.6	−9.53	NT	
<b>24<sup>a</sup></b>	1	Me	<i>t</i> -Bu	COCH <sub>2</sub> SCH <sub>2</sub> - <i>c</i> -Pr	6.4	−9.48	NT	
<b>25<sup>a</sup></b>	1	Me	<i>t</i> -Bu	COCH <sub>2</sub> SOCH <sub>2</sub> - <i>c</i> -Pr	5.4	−8.56	NT	
<b>26<sup>a</sup></b>	1	Me	<i>t</i> -Bu	COCH <sub>2</sub> SO <sub>2</sub> CH <sub>2</sub> - <i>c</i> -Pr	5.7	−8.73	NT	
<b>27<sup>a</sup></b>	1	Me	<i>t</i> -Bu	COCH <sub>2</sub> N(Me)CH <sub>2</sub> - <i>c</i> -Pr	5.6	−8.78	NT	

<sup>a</sup> Inhibitors in testing set.

SWISS-PROT<sup>27</sup> (No. P09917). Homology search for 5-LOX was carried out using the BLAST software.<sup>28</sup> Only three isoenzymes of LOXs, namely rabbit reticulocyte 15-lipoxygenase (15-LOX, PDB entry 1LOX at 2.40 Å resolution),<sup>29</sup> soybean lipoxygenase-3 (PDB entry 1IK3), and soybean lipoxygenase-1 (PDB entry 1YGE), were found with sequence similarities of 40.68%, 32.35%, and 31.82%, respectively, to the target protein 5-LOX. Multiple sequence alignment was then performed among the four proteins (Figure S1, supplementary data), and the X-ray crystal structure of 15-COX was used as a template for creating an initial 3D model of 5-LOX.

## 2.2. Generation of initial models

The missing atoms of residues 210, 211, 601, 602, and 177–187 of 15-LOX in its crystal structure were added with the Loop/Search module of InsightII,<sup>30</sup> followed by a loop relaxing. Then 10 3D models of 5-LOX were generated based on the coordinates of 15-LOX using MODELLER,<sup>31</sup> and all these 3D structures were optimized with conjugate gradient minimization scheme followed by a restrained simulated annealing molecular dynamics simulation. The model with the lowest value of the objective function was selected as a representative model for further study. For COX-2, the initial model is the crystal structure of mouse fibroblast cyclooxygenase-2 complex with the inhibitor SC-558 retrieved from the Brookhaven Protein Data Bank (PDB entry: 6COX).

## 2.3. Model equilibration by molecular dynamics

To further equilibrate the 3D model, a 4-ns MD simulation was performed using program AMBER 7.0 by the enzyme solvated in a  $97.9 \times 84.8 \times 84.3 \text{ Å}^3$  rectangular box filled with 16713 TIP3P water molecules,<sup>32</sup> followed by an additional structural relaxation. The system was initially heated to 300 K with a 5 ps time interval per 100 K. During the simulation, eight torsion angle and 16 pairwise  $\text{N}^{\text{e}}-\text{N}^{\text{e}}$  and  $\text{N}^{\text{e}}-\text{O}$  NMR distance restraints for iron center, including three histidines (His367, His372, and His550) and the C-terminus Ile673, were generated as additional input information for the SANDER program in AMBER 7.0,<sup>33</sup> which kept these four ligand residues arranged as a distorted octahedron with two adjacent, unoccupied positions.<sup>34</sup> Integration time step was set as 2 fs, the non-bonded cutoff was set to 10.0 Å, and all bonds involving hydrogen were constrained using the SHAKE algorithm.<sup>35</sup> The overall quality of the final model was assessed by using the Procheck<sup>36</sup> program and the Profile-3D<sup>37,38</sup> and Prostat module of InsightII.

## 2.4. Binding free energy

Initial structures of 27 DHDMBF analogues (Table 1) were generated by Sybyl,<sup>39</sup> which were subsequently optimized using the Powell method with Tripos force field<sup>40</sup> and Gasteiger–Marsilli charges.<sup>41–43</sup> Then, AutoDock 3.0.3<sup>44,45</sup> was used to predict the binding free energies ( $\Delta G$ s) of the compounds to COX-2 and 5-LOX, respectively, using the Lamarckian genetic algorithm

(LGA)<sup>45</sup> with the same parameter settings described in our previous study.<sup>46</sup>

## 2.5. 3D-QSAR analyses

To build predictive QSAR models for designing dual functional inhibitors against both COX-2 and 5-LOX, 21 DHDMBF analogues with dual inhibitory activities were selected to perform CoMFA<sup>47</sup> and CoMSIA<sup>47</sup> analyses based on the binding conformations derived from the molecular docking simulations. The parameters for CoMFA and CoMSIA are the same as our previous study.<sup>48</sup> To verify the constructed models further, six compounds were used to compose a testing set.

# 3. Results and discussion

## 3.1. 5-LOX model

Figure 1 depicts the alignment between the constructed 5-LOX and the template rabbit 15-LOX (Figure S1, Supplementary data). Iron ligand residues crucial for activity of the human 5-LOX, as shown in Figure 1, were correctly aligned as reported.<sup>49</sup> The 4 ns MD simulation shows that the constructed 3D model takes about 2 ns for equilibration, with a root-mean square deviation (RMSD) of 2.3 Å for the backbone and 2.8 Å for all atoms, respectively, in comparison with the initial structure (Figure S2, Supplementary data). The Profile-3D compatibility scores for the initial and final 3D models are 203.52 and 232.50, respectively (Figure S3, Supplementary data). The high score of the final model also indicates high reliability of the model. Figure 2 shows the final model of 5-LOX and, for comparison, the structure of the template 15-LOX (1LOX). It was observed that both structures share a similar feature, especially, those helices near the iron center are almost identical.

Further checked by Procheck<sup>36</sup> and Prostat, the final 5-LOX model (after equilibrium and re-minimization) shows that more than 91.8% residue  $\phi-\psi$  angles are in the ‘core’ regions of Ramachandran plot (Figure S4, Supplementary data), and the overall  $G$ -factor<sup>50</sup> is  $-0.03$ , indicating again that the final 3D model of 5-LOX is acceptable. Moreover, residues located in the unfavorable regions are far from the substrate-binding domain, indicating that these residues may not affect the ligand–protein-binding simulations.

## 3.2. Interactions between inhibitors and receptors

Figure 3 shows the conformational superposition of SC-558 (1-phenylsulfonamide-3-trifluoromethyl-5-para-bromophenylpyrazole, a selective inhibitor of COX-2) from the X-ray crystal structure of SC-558–COX-2 complex and that from the docking calculation. The RMSD between the two conformations is only 0.45 Å, indicating that the parameter set for docking is capable of reproducing the X-ray structure. The predicted binding free energies ( $\Delta G$ s) for all the DHDMBFs to COX-2 and to 5-LOX are listed in Table 1. A linear



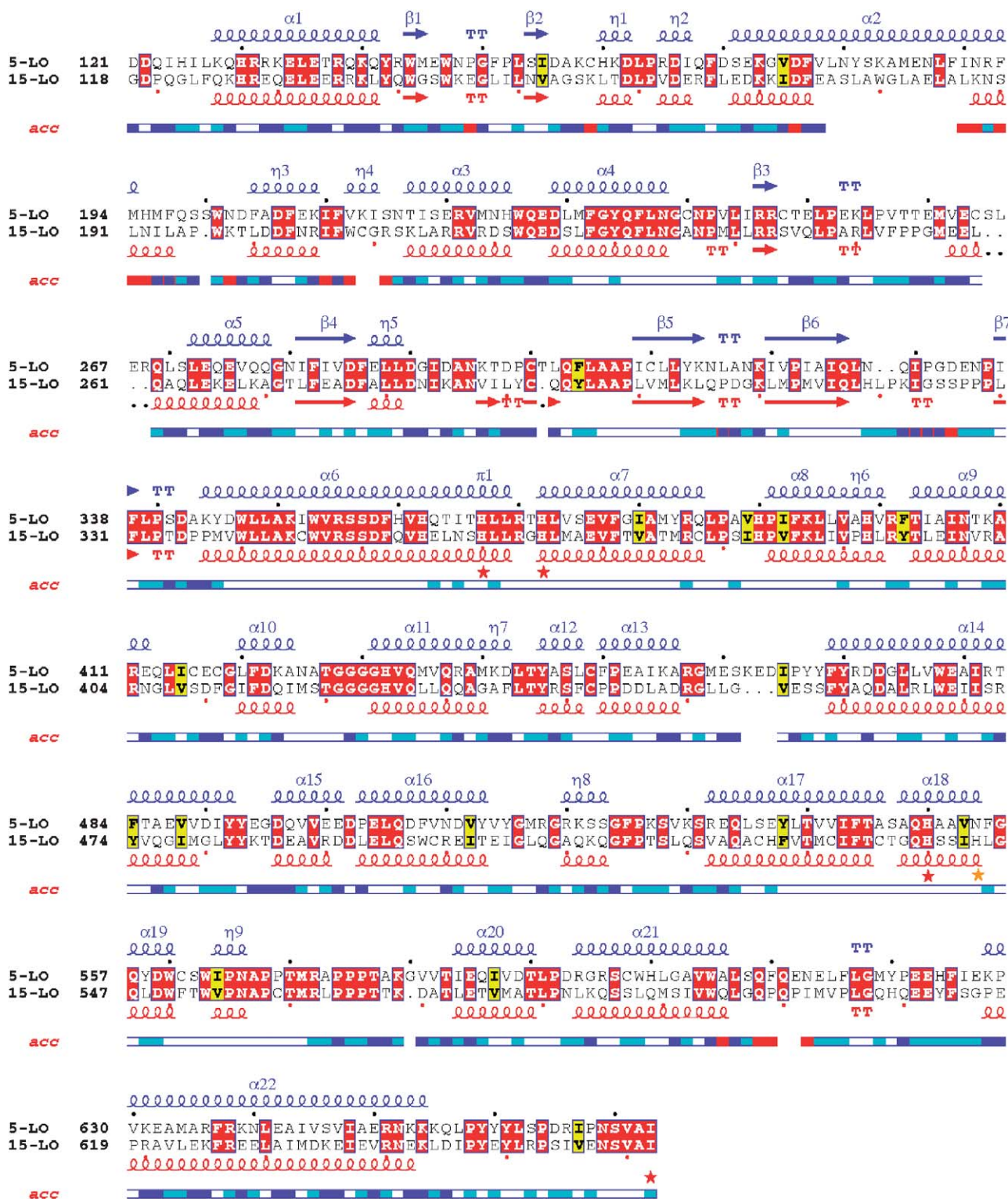


**Figure 1.** Structure-based sequence alignment of the family of lipoxygenases. A red box means strict identity, and a yellow box indicates similarity within a group. Members of the lipoxygenase family are compared with the secondary structure elements of rabbit reticulocyte 15-LOX: helices with squiggles, beta strands with arrows, and turns with TT letters. Accessibility of 15-LOX is rendered by a bar above: blue is accessible, cyan is intermediate, white is buried, and red is not predicted. The iron ligands are marked by a red star under the sequence. Figure was prepared using the ESPrnt program.<sup>52</sup>

regression analysis reveals good correlations between the experimental inhibitory potencies ( $-\log IC_{50}$ ) of the DHDMBF analogues and the predicted  $\Delta G$ s to the

two enzymes, the  $r^2$  values are 0.721 and 0.588 for COX-2 and 5-LOX, respectively (Eqs. 1 and 2, and Fig. 4). These correlations demonstrate that the binding

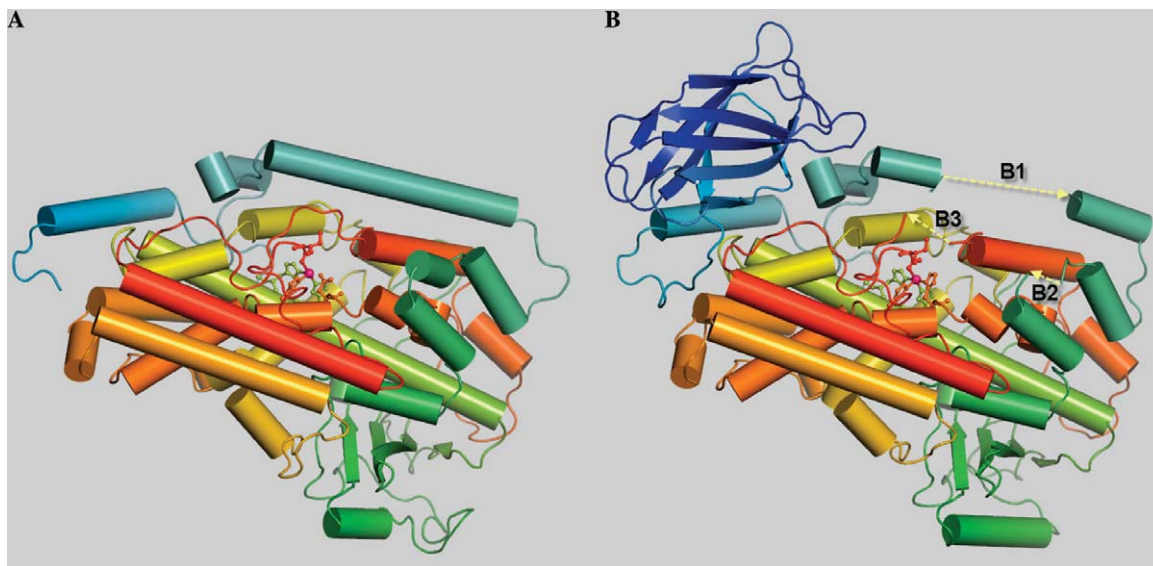


**Figure 2.** Comparison of the secondary structure of 5-LOX model (A) with that of the 15-LOX crystal structure (B).  $\alpha$ -Helices are represented as cylinders,  $\beta$ -sheets as flat ribbons, and coils as strands. The non-heme iron and its ligand residues are shown in sticks. Missing residue segments 176–186, 209–210, and 600–601 in 5-LOX are labeled as B1, B2, and B3, respectively. Each secondary structural element in 5-LOX is denoted the same color as the corresponding part of 15-LOX.

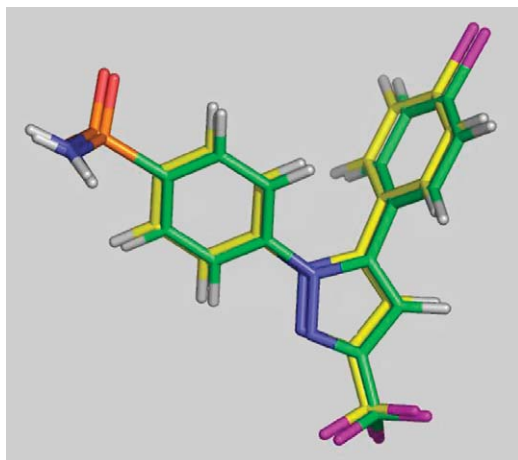


**Figure 3.** Conformational comparison of SC-558 from the crystal structure of SC-338-COX-2 complex (yellow) and that from the docking simulation (green).

conformations and binding models of the dual inhibitors to COX-2/5-LOX are reasonable:

$$-\log \text{IC}_{50}^{\text{COX-2}} = -3.487 - 0.961 \times \Delta G_{\text{COX-2}} \\ (n = 27, r^2 = 0.722, F = 68.39, s = 0.629), \quad (1)$$

$$-\log \text{IC}_{50}^{5\text{-LOX}} = -2.990 - 0.963 \times \Delta G_{5\text{-LOX}} \\ (n = 21, r^2 = 0.588, F = 27.11, s = 0.268). \quad (2)$$

Figure 5 shows two sets of alignments of the binding conformations of DHDMBF analogues, to 5-LOX

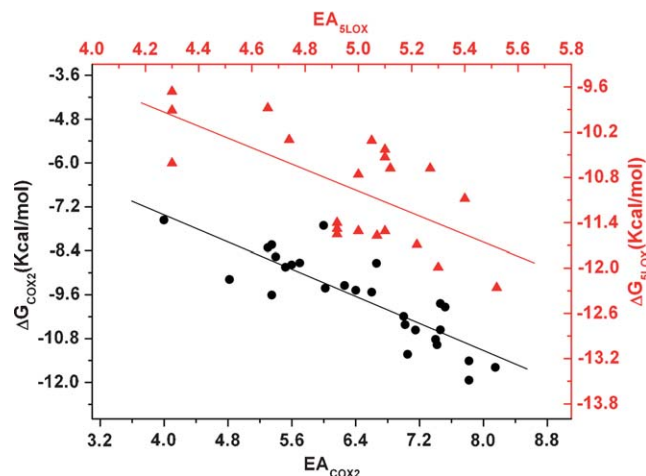


**Figure 4.** Correlation of the predicted binding free energies ( $\Delta G$ , kcal/mol) of DHDMBF analogues with COX-2 and 5-LOX to the experimental activities ( $-\log \text{IC}_{50}$ , EA). (●)  $\Delta G_{\text{COX-2}}$  vs.  $\text{EA}_{\text{COX-2}}$ , which are shown in the bottom-left coordinate system. (▲)  $\Delta G_{5\text{-LOX}}$  vs.  $\text{EA}_{5\text{-LOX}}$ , which are shown in the up-right coordinate system.

and COX-2, respectively. The overall alignment in COX-2-binding site consists of a triangle, with two bottom angles formed by *tert*-butyl and 3,3-dimethyl moieties (PA3 in Fig. 5A), and an apical angle by various 5-substituents (PA1). Unlikely, the alignment of the binding conformations of the inhibitors in 5-LOX resembles a U-shaped long thin cavity of the binding pocket.<sup>51</sup> Although most of 5-keto substituents point toward the left side (PB4 in Fig. 5B), some of them orient toward the entrance of the binding site of 5-LOX. Hence, detailed analysis about interactions between DHDMBF analogues and the binding sites of the two proteins is required for designing potent dual functional inhibitors against the two enzymes.



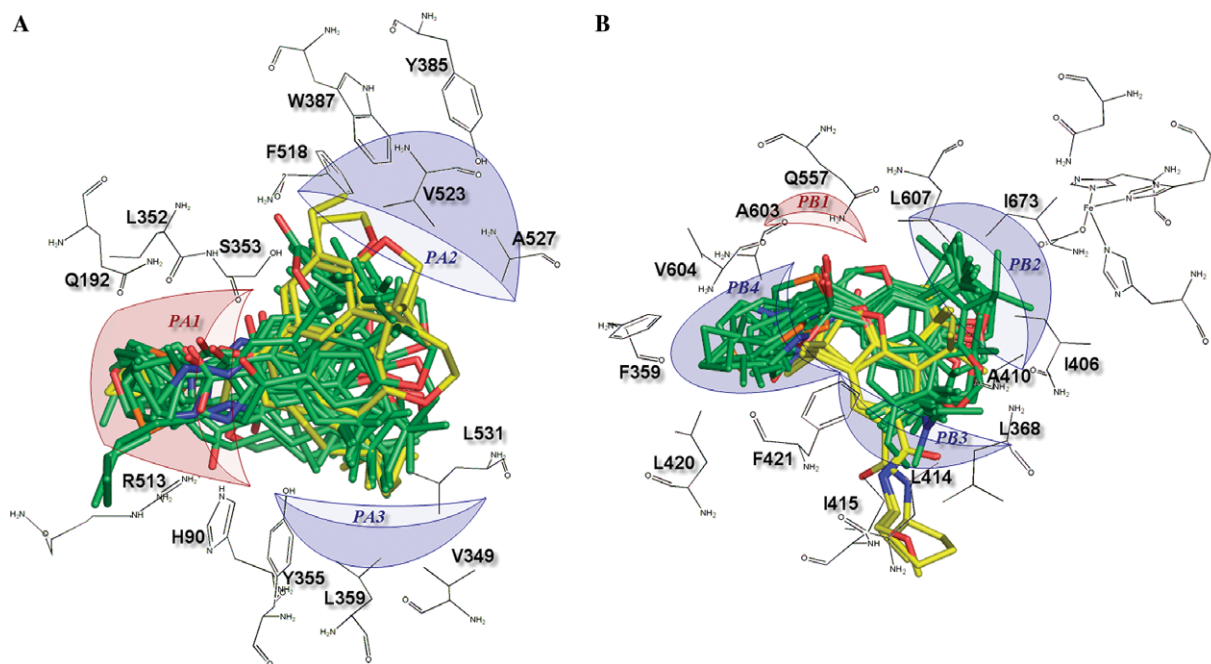


**Figure 5.** Superimposition of the binding conformations of DHDMBF analogues in the sites of COX-2 (A) and 5-LOX (B). Sketches of COX-2 and 5-LOX sub-pockets are also reported.

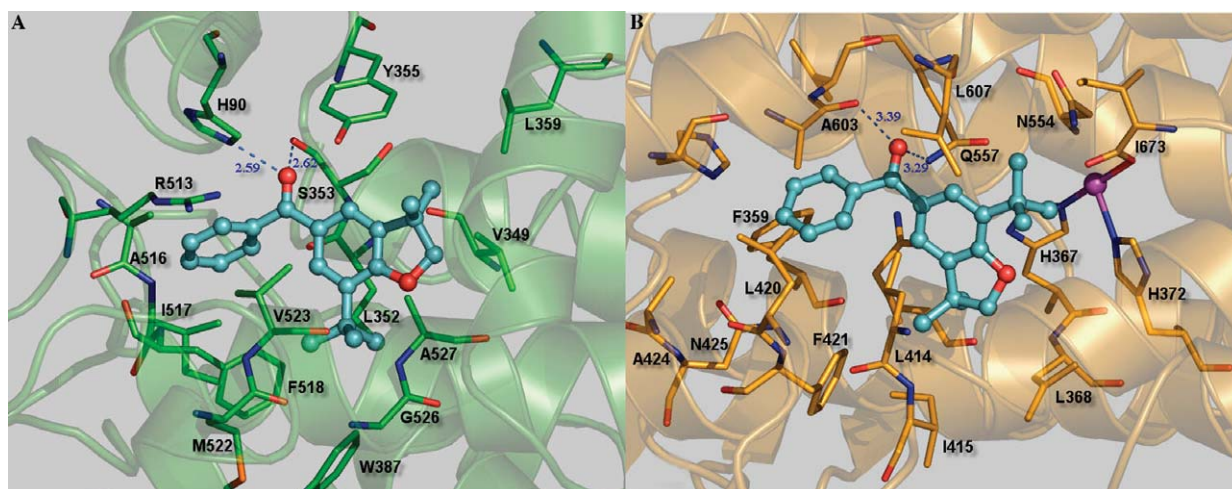
### 3.3. Interactions between inhibitors and COX-2

Figure 6A represents the 3D model of inhibitor–COX-2 complex. For clarity, only compound **3** was displayed as it is the most potent COX-2 inhibitor and exhibits balanced 5-LOX inhibitory activity as well. In general, the DHDMBF analogues are composed of two moieties, a benzo-ring and a 5-substituent. The latter can be further divided into two parts: a polar “anchor” (e.g., carbonyl, amide, amino or hetero ring structure) and a hydrophobic tail. It was found that the phenyl “tail” of compound **3** interacts with hydrophobic residues Ala516, Ile517, Phe518, and Val523 of COX-2. While its carbonyl oxygen takes such an orientation that forms two hydrogen bonds with polar residues His90 and

Ser353 with bond lengths of 2.59 and 2.62 Å, respectively.

The bulky and hydrophobic benzo-ring moiety was found to match the central hydrophobic channel well, with its  $R_1$  and  $R_2$  groups interacting with sub-pockets PA2 and PA3, respectively (Fig. 5A). Therefore, removing either  $R_1$  or  $R_2$  could reduce the hydrophobic interaction between inhibitors and the two sub-pockets. Indeed, compound **8** without  $R_1$  substituent is a much weaker inhibitor than compounds **3** and **9** with a smaller  $R_2$ .

The 5-substituent was found to interact with sub-pocket PA1 (Fig. 5A). Thus, the size and shape of its hydrophobic “tail” play an important role in determining which



**Figure 6.** The binding models of compound **3** with COX-2 (A) and 5-LOX (B). The inhibitor is represented as ball-and-stick and residues within 4 Å around the inhibitor are denoted as stick. The blue dash lines denote the hydrogen bonds.

residue to form hydrogen bonds to its ‘anchor’. Our modeling results reveal that phenyl or aliphatic chains with the length of three or four carbon atoms lead to, at least, two strong hydrogen bonds between the ‘anchor’ and residues His90 and Ser353. However, longer hydrophobic tails result in weaker hydrogen bonding. Thus, under the influence of hydrophobic tail, the polar ‘anchor’ of DHDMBF analogues determines the orientation of the benzo-ring moiety through hydrogen-bonding interactions, the strength of which is crucial to the potency of COX-2 inhibitory activity.

### 3.4. Interactions between inhibitors and 5-LOX

Figure 6B depicts the 3D model of inhibitor–5-LOX complex with compound **3** displayed as well. In agreement with the mutagenesis studies,<sup>49,51</sup> it was found through this model that the bottom of the substrate-binding pocket is defined by the side chains of Phe359, L420, Ala424, Asn425, and Ala603 (PB4, Fig. 5B). The wall of the channel is mainly lined with hydrophobic residues (PB2 and PB3, Fig. 5B), except for Asn554 and four iron ligand residues around the iron center.

In comparison of Figure 5B with A, some similar interaction features were observed. First, the polar ‘anchor’, which forms hydrogen bonds at the entrance of the sub-pocket PA1 in COX-2, also acts as a donor to form hydrogen bond in the 5-LOX-binding site. As shown in Figure 6B, the carbonyl oxygen of molecule **3** forms a hydrogen bond with the N<sup>ε2</sup> atom of Gln557. This hydrogen bond is also widely presented among other inhibitor–5-LOX complexes (Fig. 5B). Similar to the binding with COX-2, this ‘anchor’ also intensively stabilizes the inhibitors in 5-LOX pocket through hydrogen bonding and electrostatic interactions. Therefore, this ‘anchor’ is essential to a dual functional inhibitor against both COX-2 and 5-LOX. Second, the hydrophobic ‘tail’, located at the bottom of sub-pocket PA1 in COX-2, also interacts with the bottom of the binding

pocket (PB4) in 5-LOX through hydrophobic interactions. However, the PB4 is more hydrophobic than the PA1 in COX-2, consequently, leading to weaker interaction if the carboxyl group is replaced by an amide at 5-substituent moiety. Exactly, compounds **11**, **12**, and **13** with an amide group are less active (labeled yellow in Fig. 5B). Therefore, a dual inhibitor should have an anchor, with a preference of carbonyl to amide group.

In summary, a dual functional inhibitor against COX-2 and 5-LOX should share a similar binding mode though the overall shape and properties of these two pockets are rather different. A polar ‘anchor’ is essential for dual functional ligands to situate itself properly through hydrogen bonding, and a dihydrobenzofuran with moderately bulky hydrophobic group is favored for better interaction with both COX-2- and 5-LOX-binding sites.

### 3.5. CoMFA and CoMSIA

Table 2 lists all statistical indexes from CoMFA and CoMSIA. For COX-2, a two-component CoMFA model was obtained with cross-validated  $q^2$  of 0.782, conventional  $r^2$  of 0.917,  $F$  value of 99.484, and standard error  $s$  of 0.348, respectively. For 5-LOX, a one-component CoMFA model was constructed with  $q^2$ ,  $r^2$ ,  $F$ , and  $s$  of 0.634, 0.841, 100.862, and 0.132, respectively. The CoMSIA model for COX-2 was obtained with a cross-validated  $q^2$  of 0.548 for two components and a conventional  $r^2$  of 0.914. For 5-LOX, the CoMSIA model was built with a one-component model with  $q^2$  of 0.719 and  $r^2$  of 0.834. The high value of the conventional  $r^2$  relating to three different descriptor variables (steric, electrostatic, and hydrophobic) illustrates that these variables are appropriate to describe the interaction mode of DHDMBF analogues with COX-2 or 5-LOX, as well as the field properties around the inhibitors. For both COX-2 and 5-LOX, the sum of steric and hydrophobic fields in the CoMSIA model is approximately equal to the steric contribution in the corresponding CoMFA

**Table 2.** Statistical results of CoMFA and CoMSIA models based on the binding conformations of DHDMBF analogues in the COX-2- and 5-LOX-binding sites

		CoMFA		CoMSIA		
COX-2	$q^2$	0.782		0.548		
	Optimal components	2		2		
	$r^2$	0.914		0.914		
	$s$	0.354		0.354		
	$F$	95.968		96.062		
	$r^2_{\text{test}}$	0.773		0.755		
	$s_{\text{test}}$	0.316		0.338		
	Field contribution	Steric	Electrostatic	Steric	Electrostatic	Hydrophobic
5-LOX		0.521	0.479	0.149	0.598	0.253
	$q^2$	0.634		0.719		
	Optimal components	1		1		
	$r^2$	0.841		0.834		
	$s$	0.132		0.135		
	$F$	100.862		95.505		
	Field contribution	Steric	Electrostatic	Steric	Electrostatic	Hydrophobic
		0.488	0.512	0.152	0.524	0.324

model, which indicates those two models are consistent with each other. In addition, the distribution of electrostatic fields account for more than half of the total, indicating that electrostatic interaction is essential to the binding of DHDMBF analogues with COX-2 and 5-LOX. Figure 7 shows the predicted activities (PA) of the 21 compounds versus their experimental activities (EA) (supplementary data, Table S1). Taking into account both the statistical indexes and the observed correlation in Figure 7, we may conclude that the CoMFA and CoMSIA models are highly predictive. To further validate the reliability of the constructed models, the inhibitory activities of the six molecules in testing set for COX-2 inhibitors are predicted with the models, which are also indicated in Figure 7 in circle. The testing results with correlation coefficients,  $r^2_{\text{test}}$ , of 0.773 and 0.755 for CoMFA and CoMSIA models, respectively, indicate that the CoMFA and CoMSIA models is reliable, and could be used in designing new dual functional inhibitors.

### 3.6. CoMFA contour maps

The CoMFA contour map for COX-2 inhibition is shown in Figure 8A, with compound 3 displayed in aid of visualization. Detrimental and beneficial steric interactions are displayed in yellow and green contours, respectively, while blue and red contours illustrate the regions of desirable positive and negative electrostatic interactions. A large region of green contour around the  $R_2$  group of DHDMBF suggests that more bulky substituents in these positions will significantly improve the biological activities. Figure 7A suggests this improvement might be achieved through a hydrophobic interaction between the bulky group and the site formed by hydrophobic residues Phe518, Met522, Val523, Gly526, and Ala527. This also explains why compound 9 ( $R_2 = \text{Et}$ ) has a relatively weak COX-2 inhibitory activity (Table 1). Another green zone can be found close to the end of  $R_3$  group, hydrophobic tails of DHDMBF analogues. This steric favorable region could

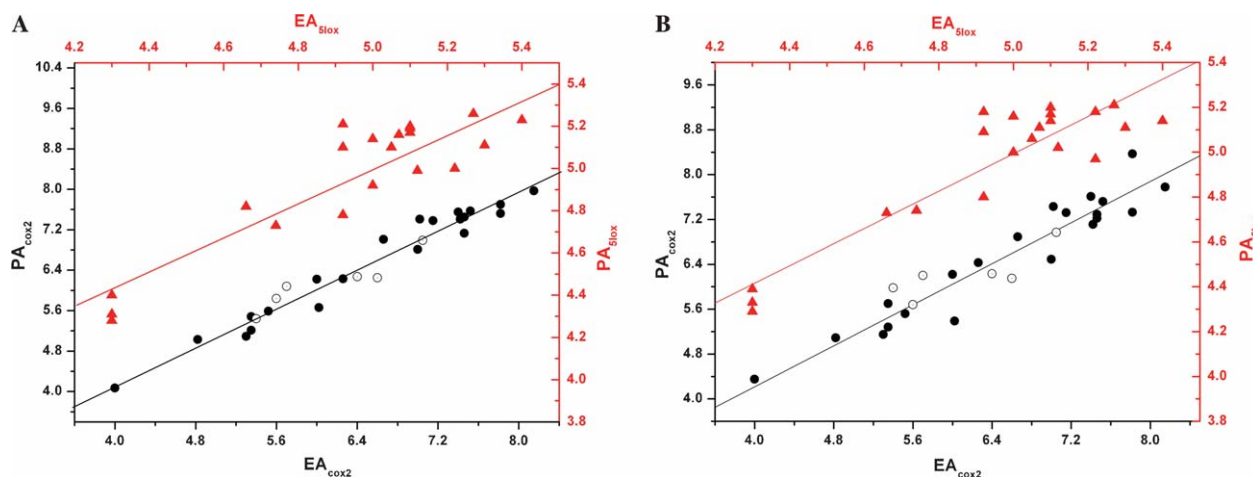


**Figure 7.** Correlation between the predicted activities (PA) of DHDMBF analogues by CoMFA (A) and CoMSIA (B), and the experimental activities ( $-\log \text{IC}_{50}$ , EA). (●)  $\text{PA}_{\text{COX-2}}$  vs.  $\text{EA}_{\text{COX-2}}$ , which are shown in the bottom-left coordinate systems. (▲)  $\text{PA}_{5\text{-LOX}}$  vs.  $\text{EA}_{5\text{-LOX}}$ , which are shown in the up-right coordinate systems. (○) Values for compounds in the testing set.

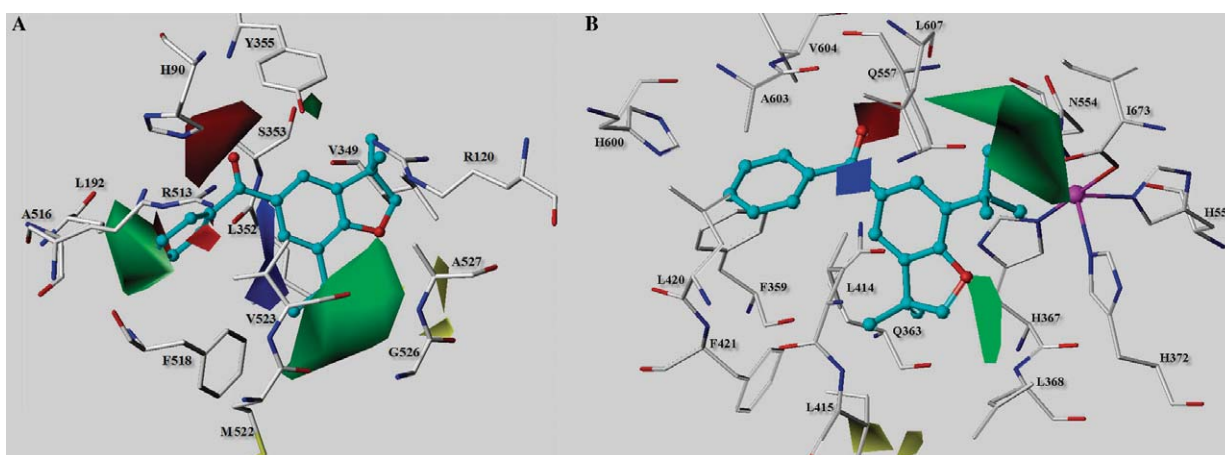


**Figure 8.** CoMFA contour maps as compared with the topology of 3-COX-2 complex (A) and 3-5-LOX complex (B). Residues within 4 Å around the inhibitor are shown. The residues are represented as sticks, and inhibitors are shown in ball-and-stick. For the contour maps steric favored areas are in green; steric unfavored areas are in yellow; positive charge-favored areas are in blue; positive charge unfavored areas in red.



be related to the hydrophobic interaction with the bottom of COX-2 sub-pocket PA1, as discussed in the previous binding mode studies. Compounds with higher COX-2 inhibitory activities, for example, **1**, **3**, and **18**, generally bear a bulky group at this position. The red polyhedron locates around the carbonyl oxygen of the inhibitors, which accords with earlier binding mode analyses that this structural feature acts as an ‘anchor’ to determine the orientation of DHDMBF analogues in COX-2-binding site through hydrogen-bonding interactions. The consistency between the CoMFA field distribution and the structural topological properties of the COX-2-binding site demonstrates again the reasonability of the CoMFA results.

The CoMFA map for 5-LOX inhibition is depicted in Figure 8B using the same set of color denotations as that for COX-2 with compound **3** displayed to aid visualization. Similar to the CoMFA result for COX-2, a large green zone is also present around the R<sub>2</sub> group. Associated with the feature of 5-LOX-binding site, the bulky 7-*tert*-butyl moiety of DHDMBFs facilitates the hydrophobic interaction with the region defined by residues Asn554, Leu607, and Ile673 nearby the iron center. The presence of a red contour close to the carbonyl oxygen and blue contour around the carbonyl carbon emphasizes the importance of polar ‘anchor’ in DHDMBF structures. However, there is no green contour in Fig. 8B around the hydrophobic tail of the ligand in comparison with that in Fig. 8A, indicating that too bulky substituent at this position results in a weaker molecular inhibitory activity against 5-LOX. Therefore, a dual functional ligand must have an appropriately sized group at this position.

On the basis of the two CoMFA maps, some common features for inhibiting COX-2 and 5-LOX were revealed, e.g., both the steric favorable region around group R<sub>2</sub> and the negative charge favorable region near the carbonyl group of DHDMBF analogues should be crucial for designing potent dual inhibitors against the two enzymes.

#### 4. Conclusions

The last century had witnessed remarkable progress in the development of NSAIDs, and the discovery in the early 1990s of COX-2 revitalized this field. However, by no means is the selective COX-2 inhibitor an end of the miracle. Undoubtedly, the recent new perspective on the 5-LOX pathway is likely to fuel another explosion of NSAIDs discovery, and people might expect the new generation COX-2/5-LOX dual inhibitors to take a lead.

In this study, 21 DHDMBF analogues were chosen for investigating the inhibitory mechanism against both COX-2 and 5-LOX, and for constructing highly predictive 3D-QSAR models, to provide useful information for designing new potent dual inhibitors as anti-inflammatory drug leads with safer properties. A 3D model of human 5-LOX was first constructed by homology mod-

eling and assessed by various methods. A good correlation between the predicted binding free energy based on the model and the experimental bioactivity further validates the reliability of the constructed 3D model of 5-LOX. Highly predictive 3D-QSAR models were then successfully set up through CoMFA and CoMSIA techniques based on the binding conformations discovered via molecular docking to the crystal structure of COX-2 and the constructed 5-LOX model, followed by a verification using six testing compounds. Furthermore, both CoMFA and CoMSIA models could be subtly mapped back to the 3D topology of the binding sites of the two enzymes. The modeling results provide a satisfactory explanation for the binding mechanism of DHDMBF analogues with the two enzymes, and 3D-QSAR models lead to a better understanding of how to design a potent dual inhibitor against the two enzymes. That is, new potent dual inhibitors should share a structural feature with both the steric favorable region around group R<sub>2</sub> and the negative charge favorable region near the carbonyl group. The 3D-QSAR models with high  $r^2$  values also provide a useful tool for quantitatively assessing the bioactivities of a newly designed dual inhibitor.

#### Acknowledgments

We thank Professor Arthur J. Olson for his kindness in offering us the AutoDock 3.0.3 program. We gratefully acknowledge financial support from National Natural Science Foundation of China (Grant 20472094), the Qi Ming Xing Foundation of Shanghai Ministry of Science and Technology (Grant 03QD14065), and Shanghai Key Basic R&D Program (Grant 05JC14092).

#### Supplementary data

Supplementary data associated with this article can be found, in the online version, at [doi:10.1016/j.bmc.2005.12.062](https://doi.org/10.1016/j.bmc.2005.12.062).

#### References and notes

1. Fiorucci, S.; Meli, R.; Bucci, M.; Cirino, G. *Biochem. Pharmacol.* **2001**, *62*, 1433.
2. Vane, J. R.; Botting, R. M. *Scand. J. Rheumatol. Suppl.* **1996**, *102*, 9.
3. Furst, D. E. *Am. J. Med.* **1999**, *107*, 18S.
4. Asako, H.; Kubes, P.; Wallace, J.; Gaginella, T.; Wolf, R. E.; Granger, D. N. *Am. J. Physiol.* **1992**, *262*, G903.
5. Wickelgren, I. *Science* **2004**, *303*, 941.
6. Spanbroek, R.; Grabner, R.; Lotzer, K.; Hildner, M.; Urbach, A.; Ruhling, K.; Moos, M. P.; Kaiser, B.; Cohnert, T. U.; Wahlers, T.; Zieske, A.; Plenz, G.; Robenek, H.; Salbach, P.; Kuhn, H.; Radmark, O.; Samuelsson, B.; Habenicht, A. J. *Proc. Natl. Acad. Sci. U.S.A.* **2003**, *100*, 1238.
7. Zhao, L.; Moos, M. P.; Grabner, R.; Pedrono, F.; Fan, J.; Kaiser, B.; John, N.; Schmidt, S.; Spanbroek, R.; Lotzer, K.; Huang, L.; Cui, J.; Rader, D. J.; Evans, J. F.; Habenicht, A. J.; Funk, C. D. *Nat. Med.* **2004**, *10*, 966.

8. Patrignani, P.; Daffonchio, L.; Hernandez, A.; De Caterina, R.; Pelosi, G.; Patrono, C. *J. Cardiovasc. Pharmacol.* **1992**, *20*, S208.
9. De Caterina, R.; Mazzone, A.; Giannessi, D.; Sicari, R.; Pelosi, W.; Lazzerini, G.; Azzara, A.; Forder, R.; Carey, F.; Caruso, D. *Biomed. Biochim. Acta* **1988**, *47*, S182.
10. Mehrabian, M.; Allayee, H.; Wong, J.; Shi, W.; Wang, X. P.; Shaposhnik, Z.; Funk, C. D.; Lusi, A. J.; Shih, W. *Circ. Res.* **2002**, *91*, 120.
11. Helgadóttir, A.; Manolescu, A.; Thorleifsson, G.; Gre-tarsdóttir, S.; Jónsdóttir, H.; Thorsteinsdóttir, U.; Samani, N. J.; Gudmundsson, G.; Grant, S. F.; Thorgeirsson, G.; Sveinbjörnsdóttir, S.; Valdimarsson, E. M.; Matthiasson, S. E.; Johannsson, H.; Gudmundsdóttir, O.; Gurney, M. E.; Sainz, J.; Thorhallsdóttir, M.; Andresdóttir, M.; Frigge, M. L.; Topol, E. J.; Kong, A.; Gudnason, V.; Hakonarson, H.; Gulcher, J. R.; Stefansson, K. *Nat. Genet.* **2004**, *36*, 233.
12. Dwyer, J. H.; Allayee, H.; Dwyer, K. M.; Fan, J.; Wu, H.; Mar, R.; Lusi, A. J.; Mehrabian, M. N. *Engl. J. Med.* **2004**, *350*, 29.
13. Ben-Asher, E.; Lancet, D. *Isr. Med. Assoc. J.* **2004**, *6*, 318.
14. Lotzer, K.; Funk, C. D.; Habenicht, A. *J. Biochim. Biophys. Acta* **2005**, *1736*, 30.
15. Gilroy, D. W.; Tomlinson, A.; Willoughby, D. A. *Eur. J. Pharmacol.* **1998**, *355*, 211.
16. Nickerson-Nutter, C. L.; Medvedeff, E. D. *Arthritis Rheum.* **1996**, *39*, 515.
17. Dyer, R. D.; Connor, D. T. *Curr. Pharm. Des.* **1997**, *3*, 463.
18. Charlier, C.; Michaux, C. *Eur. J. Med. Chem.* **2003**, *38*, 645.
19. de Leval, X.; Julemont, F.; Delarge, J.; Pirotte, B.; Dogne, J. *Curr. Med. Chem.* **2002**, *9*, 941.
20. Sietsema, W. K.; Kelm, G. R.; Deibel, R. M.; Doyle, M. J.; Loomans, M. E.; Smyth, R. E.; Kinnett, G. O.; Eichhold, T. H.; Farmer, R. W. *J. Pharm. Sci.* **1993**, *82*, 610.
21. Janusz, J. M.; Young, P. A.; Ridgeway, J. M.; Scherz, M. W.; Enzweiler, K.; Wu, L. I.; Gan, L. X.; Chen, J.; Kellstein, D. E.; Green, S. A.; Tulich, J. L.; Rosario-Jansen, T.; Magrisso, I. J.; Wehmeyer, K. R.; Kuhlbeck, D.; Eichhold, T. H.; Dobson, R. L. M. *J. Med. Chem.* **1998**, *41*, 3515.
22. Janusz, J. M.; Young, P. A.; Scherz, M. W.; Enzweiler, K.; Wu, L. I.; Gan, L. X.; Pikul, S.; McDow-Dunham, K. L.; Johnson, C. R.; Senanayake, C. B.; Kellstein, D. E.; Green, S. A.; Tulich, J. L.; Rosario-Jansen, T.; Magrisso, I. J.; Wehmeyer, K. R.; Kuhlbeck, D. L.; Eichhold, T. H.; Dobson, R. L. M. *J. Med. Chem.* **1998**, *41*, 3102.
23. Janusz, J. M.; Young, P. A.; Ridgeway, J. M.; Scherz, M. W.; Enzweiler, K.; Wu, L. I.; Gan, L. X.; Darolia, R.; Matthews, R. S.; Hennes, D.; Kellstein, D. E.; Green, S. A.; Tulich, J. L.; Rosario-Jansen, T.; Magrisso, I. J.; Wehmeyer, K. R.; Kuhlbeck, D. L.; Eichhold, T. H.; Dobson, R. L. M.; Sirko, S. P.; Farmer, R. W. *J. Med. Chem.* **1998**, *41*, 1112.
24. Klebe, G.; Abraham, U.; Mietzner, T. *J. Med. Chem.* **1994**, *37*, 4130.
25. Walther, M.; Anton, M.; Wiedmann, M.; Fletterick, R.; Kuhn, H. *J. Biol. Chem.* **2002**, *277*, 27360.
26. Hemak, J.; Gale, D.; Brock, T. G. *J. Mol. Model. (Online)* **2002**, *8*, 102.
27. Bairoch, A.; Apweiler, R. *Nucleic Acids Res.* **1999**, *27*, 49.
28. Altschul, S. F.; Gish, W.; Miller, W.; Myers, E. W.; Lipman, D. J. *J. Mol. Biol.* **1990**, *215*, 403.
29. Gillmor, S. A.; Villasenor, A.; Fletterick, R.; Sigal, E.; Browner, M. F. *Nat. Struct. Biol.* **1997**, *4*, 1003.
30. Insight II. UserGuide, MSI Inc., San Diego, USA, 2000.
31. Šali, A. *Mol. Med. Today* **1995**, *1*, 270.
32. Jorgensen, W. L. C. J.; Madura, J. D.; Impey, R. W.; Klein, M. L. *J. Chem. Phys.* **1983**, *79*, 926.
33. Pearlman, D. A.; Case, D. A.; Caldwell, J. W.; Ross, W. S.; Cheatham, T. E. I.; DeBolt, S.; Ferguson, D.; Seibel, G.; Kollman, P. *Comp. Phys. Commun.* **1995**, *91*, 1.
34. Prigge, S. T.; Boyington, J. C.; Faig, M.; Doctor, K. S.; Gaffney, B. J.; Amzel, L. M. *Biochimie* **1997**, *79*, 629.
35. Ryckaert, J. P.; Ciccotti, G.; Berendsen, H. J. C. *J. Comput. Phys.* **1977**, *23*, 327.
36. Laskowski, R. A.; Macarthur, M. W.; Moss, D. S.; Thornton, J. M. *J. Appl. Crystallogr.* **1993**, *26*, 283.
37. Bowie, J. U.; Luthy, R.; Eisenberg, D. *Science* **1991**, *253*, 164.
38. Luthy, R.; Bowie, J. U.; Eisenberg, D. *Nature* **1992**, *356*, 83.
39. SYBYL. Version 6.8; Tripos Associates; St. Louis, MO, 2000.
40. Clark, M.; Cramer, R.; Vannodenbosch, N. *J. Comput. Chem.* **1989**, *10*, 982.
41. Gasteiger, J.; Marsili, M. *Org. Magn. Reson.* **1981**, *15*, 353.
42. Marsili, M.; Gasteiger, J. *Croat. Chem. Acta* **1980**, *53*, 601.
43. Gasteiger, J.; Marsili, M. *Tetrahedron* **1980**, *36*, 3219.
44. Morris, G. M.; Goodsell, D. S.; Huey, R.; Hart, W. E.; Halliday, S.; Belew, R.; Olson, A. J. **1999**, AutoDock Version 3.0.3 The Scripps Research Institute, Molecular Graphics Laboratory, Department of Molecular Biology.
45. Morris, G. M.; Goodsell, D. S.; Halliday, R. S.; Huey, R.; Hart, W. E.; Belew, R. K.; Olson, A. J. *J. Comput. Chem.* **1998**, *19*, 1639.
46. Liu, H.; Huang, X.; Shen, J.; Luo, X.; Li, M.; Xiong, B.; Chen, G.; Shen, J.; Yang, Y.; Jiang, H.; Chen, K. *J. Med. Chem.* **2002**, *45*, 4816.
47. Cramer, R. D.; David, E. P.; Jeffrey, D. B. *J. Am. Chem. Soc.* **1988**, *110*, 5959.
48. Zuo, Z.; Luo, X.; Zhu, W.; Shen, J.; Shen, X.; Jiang, H.; Chen, K. *Bioorg. Med. Chem.* **2005**, *13*, 2121.
49. Hammarberg, T.; Zhang, Y. Y.; Lind, B.; Radmark, O.; Samuelsson, B. *Eur. J. Biochem.* **1995**, *230*, 401.
50. Engh, R. A.; Huber, R. *Acta Crystallogr. A* **1991**, *47*, 392.
51. Schwarz, K.; Walther, M.; Anton, M.; Gerth, C.; Feussner, I.; Kuhn, H. *J. Biol. Chem.* **2001**, *276*, 773.
52. Gouet, P.; Courcelle, E.; Stuart, D. I.; Metoz, F. *Bioinformatics* **1999**, *15*, 305.